IOP Publishing Journal of Physics D: Applied Physics

J. Phys. D: Appl. Phys. **50** (2017) 235303 (14pp) https://doi.org/10.1088/1361-6463/aa6fa1

Modeling of roughness effects on acoustic properties of micro-slits

S Y Song[1,2], X H Yang[2,3], F X Xin[1,2], S W Ren[1,2] and T J Lu[1,2]

[1] State Key Laboratory for Strength and Vibration of Mechanical Structures, Xi'an Jiaotong University, Xi'an 710049, People's Republic of China
[2] MOE Key Laboratory for Multifunctional Materials and Structures, Xi'an Jiaotong University, Xi'an 710049, People's Republic of China
[3] Department of Building Environment and Energy Engineering, School of Human Settlements and civil Engineering, Xi'an Jiaotong University, Xi'an 710049, People's Republic of China

E-mail: xiaohuyang@xjtu.edu.cn (X H Yang), fxxin@xjtu.edu.cn (F X Xin) and tjlu@xjtu.edu.cn (T J Lu)

Received 16 January 2017, revised 25 April 2017
Accepted for publication 26 April 2017
Published 17 May 2017

Abstract

An analytical model is developed to predict the effects of surface roughness on the acoustic properties of micro-slits. Periodic (sinusoidal) roughness distributed with relatively small amplitude on slit surface is assumed, enabling small parameter analysis. Within the incompressible creeping flow regime, the dependence of key fluidic and acoustic properties including static flow resistivity, tortuosity, effective density and compressibility on relative roughness and wave number of roughness is quantified. For validation, analytical predictions are compared with numerical simulation results based on the method of finite elements, with good agreement achieved. The presence of surface roughness is shown to increase both static flow resistivity and tortuosity, causing a significant increase in the effective density of the micro-slits, but has little effect on effective compressibility.

Keywords: acoustics properties, micro-slits, roughness effect, analytical modeling

(Some figures may appear in colour only in the online journal)

1. Introduction

The propagation of sound in a micro-slit is a fundamental problem in acoustics, serving the physical basis for characterizing sound absorbers designed with micro-slits [1] and porous media [2, 3]. These structures (e.g. micro-slit absorbers [4]) can be used as sound absorption materials in ventilation systems [5], aerocraft [6] and public buildings [7]. The problem has been extensively investigated during the past century.

The pioneering work was attributed to Rayleigh [8], who calculated the acoustic field between two parallel plates by solving Navier–Stokes equations. Under the assumptions that the viscous skin depth was a small fraction of the slit width, an approximated solution of the acoustic field was obtained. Nonetheless, although the solution has wide applicability it is unnecessarily complicated. Allard and Atalla [2] simplified the analysis by assuming that the flow was incompressible and the pressure was constant on a cross-section. By separately solving the fluid and heat transfer equations, they obtained analytical expressions of velocity components and temperature distribution. Exact solutions of sound field in uniform pores having circular, slit, rectangular and triangular cross sections were presented by Stinson and Champoux [9]. For a single slit, they considered separately and described the viscous effect and thermal effect of the sound field by an exact solution involving the hyperbolic tangent function. By introducing the concepts of tortuosity and porosity, they further analyzed the effective density and effective modulus of parallel smooth slits, as well as parallel smooth channels having other pore shapes, and validated these theoretical solutions against experimental measurements. Besides, for multiple micro-slits with varied widths distributed in parallel or series, the acoustic parameters can be determined using semi-phenomenological methods. Following Johnson *et al* [10] who defined and calculated the viscous characteristic length and tortuosity in order to determine acoustic properties in the lower- and upper- frequency limits, Allard *et al* [11] analyzed the thermal behavior of sound propagation. To determine the

necessary important acoustic parameters, Horoshenkov *et al* [12, 13] developed an analytical method to calculate the viscosity correction function in porous media with both uniform and non-uniform cross section area, where a log-normal pore size distribution was taken into consideration. Based on the two-point Pade approximation, they successfully obtained simple solutions of the viscosity correction function, which were proved to be of high accuracy in whole frequency range. Their work was considered to be quite useful because the parameters used in their solutions were routinely obtained in the characterization of porous media. Following their approach, we also tried to obtain simple solutions of the acoustic parameters of micro rough slits as functions of the basic geometrical parameters of the surface roughness. In general, for a single slit or parallel slits having the same cross-sectional area, there is an exact solution of the sound field. However, for multi slits with varying cross-sectional areas along the length, there is no exact solution. As a result, one needs to investigate the asymptotic behaviors (i.e. lower- and upper- frequency limits) of the channels first and then approximate relevant acoustic parameters for much wider frequency ranges.

Great efforts have been made to investigate sound propagation in micro-slits [1, 14–19]. Although existing models can provide accurate predictions of the acoustic properties of micro-slits, they do not take surface roughness into consideration. Previous theoretical and experimental investigations show that surface roughness can significantly affect sound propagation and fluid flow in pipes and slits [20]. In the nineteenth century, Darcy [21] introduced a dimensionless parameter, namely the Darcy friction factor, to evaluate the roughness effect on pressure drop. After a series of experimental studies on fluid flow in different kinds of rough pipes [22], the Darcy friction factor was found to be influenced by both the Reynolds number and relative roughness. Nikuradse [23] and Colebrook [24, 25] carefully conducted experiments to evaluate the influence of uniform roughness on pressure drop, and then proposed approximated equations to predict the Darcy friction factor. Based on Colebrook's equations and experimental data, Moody [26] presented a diagram, where the Darcy friction factor is expressed as a function of both the Reynolds number and relative roughness. In recent years, the flow constriction effect has been discovered from experiments and numerical simulations [20, 27, 28]. For instance, Kandlikar [29] revealed that flow inside a channel is resisted by the constricted flow diameter. Especially for larger relative roughness [30], increasing surface roughness increases pressure drop, leading to a growing Darcy friction factor.

Existing studies concerning the influence of surface roughness on flow field were rarely conducted from an acoustic perspective. Stinson and Champoux [9] theoretically investigated the influence of pore shape on sound propagation in porous media having uniform cross sections and introduced a new shape factor, which was independent of the sound frequency. This new shape factor has been widely used as an important parameter in the design of micro perforated panel [31]. Cortis *et al* [32] studied the influence of wedge-shaped microstructure on the acoustic properties of micro channels in the high frequency range. Achdous and Avellaneda [33] investigated the influence of pore-size dispersion and pore roughness on the permeability of porous media. More recently, Meng *et al* [34] calculated the acoustic field in micro tubes covered by surface-mounted fibrous roughness elements and provided approximated solutions to the velocity and temperature distributions. Imran Bashir *et al* [35] experimentally investigated the influence of periodic rectangular strips on the propagation of surface wave and demonstrated that the surfaces composed of parallel strips could be considered as locally reacting slit-pore layers. And when the strips were distinct from each other, they would behave as the surface with periodic roughness. While these models focused on particular kinds of surface roughness (e.g. wedge- or fibrous-shape), they also had quite complicated mathematical forms. In particular, the influence of wavy-shape roughness, which is believed to be more common in nature, is nonetheless analytically studied. From an engineering perspective, simple analytical expressions of the influence of surface roughness on the acoustic properties of micro-slits are preferred.

The present study aims to analyze the acoustic properties of micro-slits having periodic wavy roughness. To simplify the problem for analytical study, several assumptions are made: (1) geometrical dimension of micro-slit (sub-millimeter scale) is much smaller than the wavelength of sound wave; (2) wavy roughness is evenly distributed on the inner surface of the slit, with relatively small amplitude (so that small parameter analysis is applicable); (3) sound wave is viscous, incompressible and traveling under low Reynolds numbers (creeping flow regime, $\mathrm{Re} \ll 1$); (4) flow inside the slit is fully developed, with end correction neglected [36]. Under these assumptions, analytical models for the key acoustic parameters that govern the acoustic properties of micro-slits, including static flow resistivity, tortuosity and effective density, are developed. For validation, numerical simulations are performed with the finite element (FE) code COMSOL.

2. Descriptions of roughened micro-slit

Figure 1 illustrates schematically a single micro-slit with structured surface roughness: a, named as the diameter of the slit, is much smaller than the wavelength of sound; d, representing the length of the slit, is large enough to ensure fully developed flow in the slit; r, denoted as the amplitude of roughness, satisfies $r \leqslant 0.1a$ to ensure small relative roughness; b, defined as the wavelength of roughness, is relatively big to avoid large slope of the boundary wall (i.e. $b \gg r$). Acoustic radiation is generated by a plane wave, perpendicular to the inlet cross section of the slit (figure 1).

Surface roughness is generated in a wavy pattern, which can be characterized as:

$$\begin{aligned} Y &= a(1 - \varepsilon g(X)), \quad \text{up} \\ Y &= a(0 + \varepsilon g(X)), \quad \text{bottom} \end{aligned} \tag{1}$$

where (X, Y) are the Cartesian coordinates, ε is the relative roughness defined by $\varepsilon = r/a$, $g(X)$ is the boundary function given by $g(X) = \cos(\beta x/a)$, and β represents the wave number of roughness, given by $\beta = 2\pi a/b$.

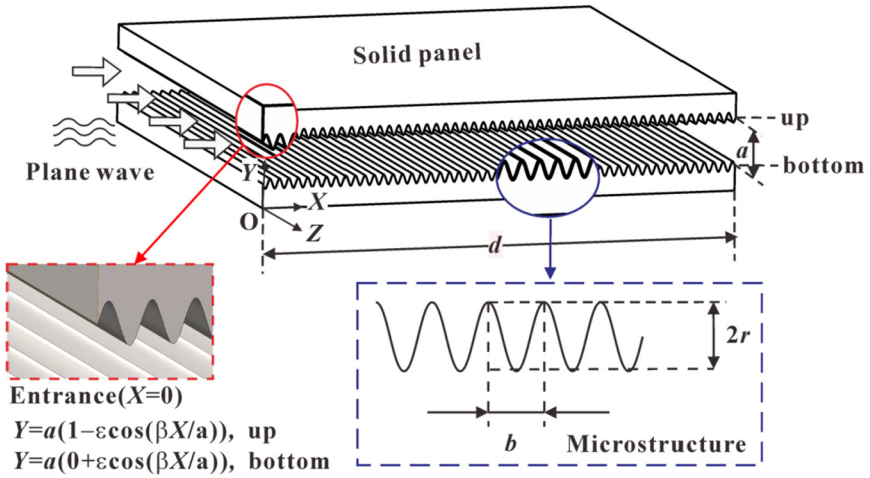

Figure 1. Illustration of a micro-slit covered by wavy roughness.

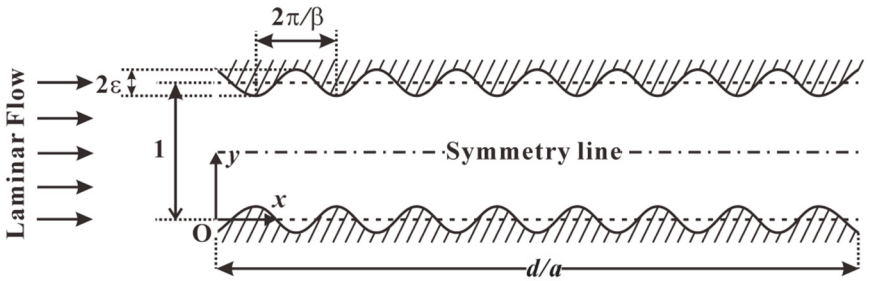

Figure 2. Sketch of a micro-slit with wavy roughness.

3. Analytical model

For sound absorbing porous media, effective density and effective compressibility are two of the most important macroscopic acoustic parameters, which are usually very difficult to be determined by direct calculations of the acoustic field. Often, approximation (semi-phenomenological) models such as that proposed by Johnson I [10] are employed, which usually consist of two parts. The first part determines key acoustic parameters in the low and high frequency limits, while the second part takes these limits into fitting functions to obtain approximate solutions of effective density and effective compressibility for porous media. Such an approach is adopted in the present study.

In section 3.1, solutions for flow field and static flow resistivity of rough micro-slit in static incompressible creeping flow are obtained using the perturbation method [37–44]. Tortuosity is determined in static incompressible inviscid flow with the small parameter method [40] in section 3.2. In section 3.3, effective density and effective compressibility are obtained using the semi-phenomenological model of Johnson *et al* [10].

3.1. Viscous flow field and static flow resistivity

Static flow resistivity in a rough micro-slit can be measured in static incompressible creeping flow and defined by [2, 45]

$$\sigma = \frac{\Delta P}{dU} \tag{2}$$

where σ is the static flow resistivity, ΔP is the pressure drop across the slit, d is the length of the slit (figure 1), and U is the volume average velocity (i.e. the average velocity of the fluid flow in a unit cell).

According to equation (2), the exact values of average velocity and pressure drop are necessary for the calculation. In this study, with small relative roughness assumed (i.e. $\varepsilon \ll 1$), the flow field is obtained by solving the dimensionless Stokes equations using the perturbation method [41, 42]. Detailed description of the non-dimensional treatment for the system is presented in the appendix. With reference to figure 2, the Stokes equation in dimensionless form is:

$$0 = -\nabla p + \nabla^2 \mathbf{u} \tag{3}$$

$$\begin{cases} u = v = 0, & \text{at } y = \varepsilon g(x) \\ \dfrac{\partial u}{\partial y} = v = 0, & \text{at } y = \dfrac{1}{2} \end{cases} \tag{4}$$

where (x, y) are the dimensionless coordinates, u is the velocity component in x direction, and v is the velocity component in y direction.

Substitution of $u = \partial\psi/\partial y, v = -\partial\psi/\partial x$ into (3) and (4) results in:

$$\nabla^4 \psi = 0 \tag{5}$$

$$\begin{cases} \dfrac{\partial \psi}{\partial x} = \dfrac{\partial \psi}{\partial y} = 0, & \text{at } y = \varepsilon g(x) \\ \dfrac{\partial \psi}{\partial x} = \dfrac{\partial^2 \psi}{\partial y^2} = 0, & \text{at } y = \dfrac{1}{2} \end{cases} \tag{6}$$

where ψ is the stream function.

The solution to a disturbed system can be expanded into a basic solution and a series of disturbed solutions, as [40–42]:

$$\psi(x, y) = \psi_0(x, y) + \varepsilon \psi_1(x, y) + o(\varepsilon) \tag{7}$$

where ψ_0 is the zero order solution and ψ_1 is the first order solution. For simplicity, only the first order approximation is considered in the present study. In order to qualify the disturbance source, it is necessary to revise the boundary condition, i.e. equation (6) at $y = \varepsilon g(x)$, by taking Taylor expansion of $\psi(x, y)$, as:

$$\psi(x, y)\big|_{y=\varepsilon g(x)} = \psi_0(x, y)\big|_{y=0} + \varepsilon \left(g(x) \frac{\partial \psi_0(x, y)}{\partial y}\bigg|_{y=0} + \psi_1(x, y)\big|_{y=0} \right) + o(\varepsilon). \tag{8}$$

The two terms, $\partial\psi/\partial x\big|_{y=\varepsilon g(x)}$ and $\partial\psi/\partial y\big|_{y=\varepsilon g(x)}$, in (6) can be treated in a similar manner. Substitution of (7) into (5) yields:

$$\nabla^4 \psi_0 + \varepsilon \nabla^4 \psi_1 + o(\varepsilon) = 0. \tag{9}$$

According to the order of the small parameter ε, (9) can be decomposed into two independent equations, namely, the zero- and first-order equations. The zero-order governing equations are given by:

$$\nabla^4 \psi_0 = 0$$
$$\begin{cases} \dfrac{\partial \psi_0}{\partial x} = 0, \dfrac{\partial \psi_0}{\partial y} = 0 & \text{at } y = 0 \\ \dfrac{\partial \psi_0}{\partial x} = \dfrac{\partial^2 \psi_0}{\partial y^2} = 0 & \text{at } y = \dfrac{1}{2} \end{cases} . \tag{10}$$

In dimensionless coordinates, the volume average velocity has a magnitude of unity. Therefore, the basic solution is $\psi_0 = 3y^2 - 2y^3$, resulting in $u_0 = 6y(1 - y)$.

The first-order governing equations are:

$$\nabla^4 \psi_1 = 0$$
$$\begin{cases} \dfrac{\partial \psi_1}{\partial x} = 0, \dfrac{\partial \psi_1}{\partial y} = -6g(x) + q(x, \varepsilon, \beta) & \text{at } y = 0 \\ \dfrac{\partial \psi_1}{\partial x} = \dfrac{\partial^2 \psi_1}{\partial y^2} = 0 & \text{at } y = \dfrac{1}{2} \end{cases} \tag{11}$$

where $q(x, \varepsilon, \beta)$ is an additional term introduced to account for flow constriction effect, which is a function of position x, relative roughness ε and wave number of roughness β. The flow constriction effect represents the reduction of hydraulic radius in the micro-slit due to surface roughness. To simplify the analysis, $q(x, \varepsilon, \beta)$ is replaced below by its integral average value in x direction, $Q(\varepsilon, \beta) = \frac{\beta}{2\pi} \int_0^{2\pi/\beta} q(x, \varepsilon, \beta) \mathrm{d}x$.

To separate x and y in equation (11), the Fourier transform of ψ_1 in x direction is performed:

$$\psi_1 = \sum_{k=-\infty}^{\infty} \varphi_k(y) \mathrm{e}^{jk\beta x} \tag{12}$$

where $\varphi_k(y)$ is the Fourier expansion of ψ_1. Substitution of (12) into (11) results in:

$$\sum_{k=-\infty}^{\infty} \nabla^4 (\varphi_k(y) \mathrm{e}^{jk\beta x}) = 0$$
$$\begin{cases} \dfrac{\partial}{\partial x}\left(\sum\limits_{k=-\infty}^{\infty} \varphi_k(y) \mathrm{e}^{jk\beta x} \right) = 0, \dfrac{\partial}{\partial y}\left(\sum\limits_{k=-\infty}^{\infty} \varphi_k(y) \mathrm{e}^{jk\beta x} \right) = -3\mathrm{e}^{-\beta x} - 3\mathrm{e}^{\beta x} + Q\mathrm{e}^0 & \text{at } y = 0 \\ \dfrac{\partial}{\partial x}\left(\sum\limits_{k=-\infty}^{\infty} \varphi_k(y) \mathrm{e}^{jk\beta x} \right) = \dfrac{\partial^2}{\partial y^2}\left(\sum\limits_{k=-\infty}^{\infty} \varphi_k(y) \mathrm{e}^{jk\beta x} \right) = 0 & \text{at } y = \dfrac{1}{2} \end{cases} . \tag{13}$$

According to the boundary condition at $y = 0$ in (13), only the terms of $k = -1, 0, 1$ exist:

$$\psi_1 = \varphi_1(y) \mathrm{e}^{j\beta x} + \varphi_{-1}(y) \mathrm{e}^{-j\beta x} + \varphi_0(y) \tag{14}$$

where $(\varphi_1(y) \mathrm{e}^{j\beta x} + \varphi_{-1}(y) \mathrm{e}^{-j\beta x})$ quantifies the periodic fluctuation of the flow field and $\varphi_0(y)$ quantifies the overall deviation of the flow field. Equation (13) can be separated into two independent equations. For $k = -1, 1$:

$$\frac{\partial^4 \varphi_1}{\partial y^4} - 2\beta^2 \frac{\partial^2 \varphi_1}{\partial y^2} + \beta^4 \varphi_1 = 0$$
$$\begin{cases} \varphi_1 = 0, \dfrac{\partial \varphi_1}{\partial y} = -3, & \text{at } y = 0 \\ \varphi_1 = 0, \dfrac{\partial^2 \varphi_1}{\partial y^2} = 0, & \text{at } y = 1/2 \end{cases} \tag{15}$$

For $k = 0$:

$$\frac{\partial^4 \varphi_0}{\partial y^4} = 0$$
$$\begin{cases} \dfrac{\partial \varphi_0}{\partial y} = Q, & \text{at } y = 0 \\ \dfrac{\partial \varphi_0^2}{\partial y^2} = 0, & \text{at } y = 1/2. \end{cases} \tag{16}$$

The solution of (15) is given by:

$$\varphi_1(y) = \frac{3}{2\beta - \mathrm{e}^{\beta} + \mathrm{e}^{-\beta}} [(-1 + (1 - \mathrm{e}^{-\beta})y)\mathrm{e}^{\beta y} + (1 + (\mathrm{e}^{\beta} - 1)y)\mathrm{e}^{-\beta y}] \tag{17}$$

where, according to the symmetry of $\varphi_1(y)$ and $\varphi_{-1}(y)$, one has $\varphi_1(y) = \varphi_{-1}(y)$.

The solution of (16) is given by:

$$\varphi_0(y) = -\frac{2}{3} R y^3 + R y^2 + Q y \tag{18}$$

where Q and R are two unknown functions of β and ε. With ε taken as a constant, it turns $R = R(\beta)$ and $Q = Q(\beta)$. Flow conservation dictates that:

$$\int_0^{2\pi/\beta}\left[\int_0^{1/2}\left(\frac{\mathrm{d}\varphi_0}{\mathrm{d}y}+\frac{\mathrm{d}\varphi_1(y)}{\mathrm{d}y}\mathrm{e}^{j\beta x}+\frac{\mathrm{d}\varphi_{-1}(y)}{\mathrm{d}y}\mathrm{e}^{-j\beta x}\right)\mathrm{d}y\right]\mathrm{d}x=0 \tag{19}$$

where $\int_0^{2\pi/\beta}\left[\int_0^{1/2}\left(\frac{\mathrm{d}\varphi_1(y)}{\mathrm{d}y}\mathrm{e}^{j\beta x}+\frac{\mathrm{d}\varphi_{-1}(y)}{\mathrm{d}y}\mathrm{e}^{-j\beta x}\right)\mathrm{d}y\right]\mathrm{d}x$ is zero because of the integration property of trigonometric function. Substitution of (18) into (19) then yields:

$$R(\beta) = -3Q(\beta). \tag{20}$$

In equation (11), an additional function $q(x, \varepsilon, \beta)$ is introduced without adding new equations and hence there lacks a boundary condition to determine the final solution of the flow field. An approximation method is proposed to solve the problem, as demonstrated below.

As the wave number of surface roughness is varied, there are two limits of viscous resistivity, corresponding separately to $\beta \to 0$ and $\beta \to \infty$. When $\beta \to 0$, the wavy roughness is distributed sparsely. As a result, due to a decline in the boundary area, the gradient of viscous stress is minimized, resulting in $(-\nabla^2 u)\big|_{\min} = (-\nabla^2 u)\big|_{\beta\to 0}$. In sharp contrast, when $\beta \to \infty$, the wavy roughness is distributed densely, thus preventing the flow from passing near the boundary. Correspondingly, the gradient of viscous stress near the boundary is maximized, causing $(-\nabla^2 u)\big|_{\max} = (-\nabla^2 u)\big|_{\beta\to\infty}$. As the wavy roughness can hinder the flow, $(-\nabla^2 u(\beta))$ is assumed to be monotonic increasing function of β so that $\frac{\partial}{\partial\beta}(-\nabla^2 u) > 0$. With reference to (7) and (14), it turns out that $\frac{\partial}{\partial\beta}\left[-\frac{\partial^3\varphi_0}{\partial y^3}\right] > 0$ and hence $\frac{\partial R}{\partial\beta} > 0$. As logistic function [46, 47] satisfies most of the properties of $R(\beta)$, it is reasonable to adopt logistic regression to fit $R(\beta)$ and $Q(\beta)$:

$$R(\beta) = \left(R_1\frac{2\mathrm{e}^{-\frac{1}{5\pi}\beta}}{1+\mathrm{e}^{-\frac{1}{5\pi}\beta}}+R_2\right) \tag{21}$$

$$Q(\beta) = \left(Q_1\frac{2\mathrm{e}^{-\frac{1}{5\pi}\beta}}{1+\mathrm{e}^{-\frac{1}{5\pi}\beta}}+Q_2\right) \tag{22}$$

where R_1, R_2, Q_1 and Q_2 are four constants to be determined.

When $\beta \to \infty$, the flow field may be determined by considering an analogue with laminar flow in a smooth slit of diameter $(1 - 2\varepsilon)$, leading to:

$$u_{\beta\to\infty} = \frac{6(y-\varepsilon)(1-\varepsilon-y)}{(1-2\varepsilon)^3}. \tag{23}$$

Flow conservation requires $\int_0^{2\pi/\beta} u\mathrm{d}x = \int_0^{2\pi/\beta} u_{\beta\to\infty}\mathrm{d}x$, from which:

$$R_2 = \frac{3(6-12\varepsilon+8\varepsilon^2)}{(1-2\varepsilon)^3} \tag{24}$$

$$Q_2 = \frac{6(\varepsilon-1)}{(1-2\varepsilon)^3}. \tag{25}$$

When $\beta \to 0$, the flow field may be decided by an analogue with laminar flow in a slit with varying width of $(1 - 2\varepsilon\cos(\beta x))$, resulting in:

$$u_{\beta\to 0} = \frac{6(y-\varepsilon\cos(\beta x))(1-\varepsilon\cos(\beta x)-y)}{(1-2\varepsilon\cos(\beta x))^3}. \tag{26}$$

Due to flow conservation, $\int_0^{2\pi/\beta} u\mathrm{d}x = \int_0^{2\pi/\beta} u_{\beta=0}\mathrm{d}x$. It follows that:

$$R_1 = \frac{3(2\varepsilon^2+1)}{\varepsilon(1-4\varepsilon^2)^{2.5}} - \frac{3}{\varepsilon(1-2\varepsilon)^3} \tag{27}$$

$$Q_1 = \frac{24\varepsilon^3-15\varepsilon}{(1-4\varepsilon^2)^{2.5}} - \frac{6(\varepsilon-1)}{(1-2\varepsilon)^3}. \tag{28}$$

Finally, based on equations (17)–(28), the solution for velocity field in static incompressible creeping flow is obtained as:

$$\begin{aligned}
u &= 6y - 6y^2 \\
&+\varepsilon\left[\begin{array}{l} 2\left(\left(\frac{3(2\varepsilon^2+1)}{\varepsilon(1-4\varepsilon^2)^{2.5}}-\frac{3}{\varepsilon(1-2\varepsilon)^3}\right)\frac{2\mathrm{e}^{-\frac{1}{5\pi}\beta}}{1+\mathrm{e}^{-\frac{1}{5\pi}\beta}}\right. \\ \quad\left.+\frac{3(6-12\varepsilon+8\varepsilon^2)}{(1-2\varepsilon)^3}\right)\times(-y^2+y) \\ +\left(\frac{24\varepsilon^3-15\varepsilon}{(1-4\varepsilon^2)^{2.5}}-\frac{6(\varepsilon-1)}{(1-2\varepsilon)^3}\right)\frac{2\mathrm{e}^{-\frac{1}{5\pi}\beta}}{1+\mathrm{e}^{-\frac{1}{5\pi}\beta}}+\frac{6(\varepsilon-1)}{(1-2\varepsilon)^3}\end{array}\right] \\
&+\frac{6\varepsilon\cos(\beta x)}{2\beta-\mathrm{e}^{\beta}+\mathrm{e}^{-\beta}}[(1-\mathrm{e}^{-\beta})\mathrm{e}^{\beta y}+\beta(-1+(1-\mathrm{e}^{-\beta})y)\mathrm{e}^{\beta y}+(\mathrm{e}^{\beta}-1)\mathrm{e}^{-\beta y} \\
&-\beta(1+(\mathrm{e}^{\beta}-1)y)\mathrm{e}^{-\beta y}] \\
v &= \frac{12\varepsilon\beta\sin(\beta x)}{2\beta-\mathrm{e}^{\beta}+\mathrm{e}^{-\beta}}[(-1+(1-\mathrm{e}^{-\beta})y)\mathrm{e}^{\beta y}+(1+(\mathrm{e}^{\beta}-1)y)\mathrm{e}^{-\beta y}].
\end{aligned} \tag{29}$$

Static flow resistivity in the present rough slit is given by:

$$\frac{\sigma}{\sigma_0} = \left[\frac{(2\varepsilon^2+1)}{(1-4\varepsilon^2)^{2.5}}-\frac{1}{(1-2\varepsilon)^3}\right]\frac{2\mathrm{e}^{-\frac{1}{5\pi}\beta}}{1+\mathrm{e}^{-\frac{1}{5\pi}\beta}}+\frac{1}{(1-2\varepsilon)^3} \tag{30}$$

where $\sigma_0 = \frac{3\mu}{a^2}$ is the flow resistivity in a smooth slit [2].

3.2. Ideal flow field and tortuosity

According to Johnson *et al* [10], when ideal non-viscous fluid is considered, the tortuosity can be calculated as:

$$\alpha_\infty = \langle \mathbf{u}^2(M)\rangle_\mathrm{V}/\langle \mathbf{u}(M)\rangle_\mathrm{V}^2 \tag{31}$$

where α_∞ is the tortuosity, $\langle \mathbf{u}^2(M)\rangle_\mathrm{V}$ is the volume average of the square of velocity at point M and $\langle \mathbf{u}(M)\rangle_\mathrm{V}$ is the volume average of velocity. $\mathbf{u}(M)$ can be obtained by solving the potential flow problem:

$$\nabla^2\Phi = 0 \tag{32}$$

where Φ is the potential function from which $u = \partial\Phi/\partial x$ and $v = \partial\Phi/\partial y$.

Impermeable slit wall is assumed, leading to boundary condition $v/u = \partial g(x)/\partial x$. Here, for simplification of the final

Table 1. Acoustic parameters.

Acoustic parameter	Symbol	Expression
Characteristic viscous length	Λ	$\Lambda = (8\mu\alpha_\infty/\sigma)^{1/2}/\sqrt{2/3}$
Characteristic thermal length	Λ'	$\Lambda' = \pi\left(2\int_0^{\pi/2}\sqrt{1+\varepsilon^2\beta^2\sin^2(t)}\,\mathrm{d}t\right)^{-1}$
Static viscous permeability	k_0	$k_0 = \mu/\sigma$
Static thermal permeability	k_0'	$k_0' = \Lambda'^2/12$

Table 2. Material parameters.

Material parameter	Symbol	Value
Atmospheric pressure	P_0	$P_0 = 1.013\,25 \times 10^5\,\mathrm{Pa}$
Fluid density	ρ_0	$\rho_0 = 1.23\,\mathrm{kg\,m^{-3}}$
Specific heat ratio	γ	$\gamma = 1.4$
Prandtl number	Pr	Pr = 0.74
Dynamic viscosity	μ	$\mu = 1.79 \times 10^{-5}\,\mathrm{Pa\cdot s}$
Kinematic viscous coefficient	ν	$\nu = \mu/\rho_0$
Kinematic thermal coefficient	ν'	$\nu' = \nu/\mathrm{Pr}$

expressions, $g(x) = \varepsilon\cos(\beta x)$ is replaced by $g(x) = \varepsilon\sin(\beta x)$ so that:

$$\frac{v}{u} = \frac{\partial g(x)}{\partial x} = \varepsilon\beta\cos(\beta x), \quad \text{at } y = \varepsilon g(x). \tag{33}$$

Due to symmetry, the boundary condition at the central line (figure 2) is:

$$v = 0, \quad \text{at } y = 1/2. \tag{34}$$

The perturbation expansion of Φ yields:

$$\Phi = \Phi_0 + \varepsilon\Phi_1 + o(\varepsilon) \tag{35}$$

where Φ_0 and Φ_1 are zero- and first-order solutions. Substitution of (35) into (32) leads to:

$$\begin{cases} \nabla^2\Phi_0 = 0 \\ \nabla^2\Phi_1 = 0 \end{cases}. \tag{36}$$

The inlet velocity of $u_0 = 1$ and $v_0 = 0$ gives:

$$\Phi_0 = x. \tag{37}$$

The first-order solution can be obtained by solving

$$\frac{\partial^2\Phi_1}{\partial x^2} + \frac{\partial^2\Phi_1}{\partial y^2} = 0. \tag{38}$$

According to equations (33), (35) and (37), the first-order boundary condition at slit wall can be written as $\partial\Phi_1/\partial y = \beta\cos(\beta x)$. For simplification, this is approximated as:

$$\frac{\partial\Phi_1}{\partial y} = \beta\cos(\beta x), \quad \text{at } y = 0. \tag{39}$$

Note that the above approximation is valid only when the periodic roughness has a wavelength larger than amplitude, i.e. $2\pi/\beta \gg \varepsilon$.

At slit central line, the boundary condition is:

$$\frac{\partial\Phi_1}{\partial y} = 0, \quad \text{at } y = 1/2. \tag{40}$$

Taking the Fourier expansion of Φ_1 in x direction yields:

$$\Phi_1 = \sum_{k=-\infty}^{\infty}\zeta_k(y)\mathrm{e}^{\mathrm{i}k\beta x}. \tag{41}$$

According to the boundary condition of (39), only the terms of $k = -1, 1$ remain, namely:

$$\Phi_1 = \zeta_1(y)\mathrm{e}^{\mathrm{i}\beta x} + \zeta_{-1}(y)\mathrm{e}^{-\mathrm{i}\beta x}, \quad \zeta_1(y) = \zeta_{-1}(y). \tag{42}$$

In general, as inviscid flow is assumed, no flow constriction effect is in force. Substitution of (42) into (38)–(40) gives rise to:

$$\begin{aligned} &-\beta^2\zeta_1(y) + \frac{\partial^2\zeta_1(y)}{\partial y^2} = 0 \\ &\begin{cases} \dfrac{\partial\zeta_1}{\partial y} = \dfrac{1}{2}\beta, & \text{at } y = 0 \\ \dfrac{\partial\zeta_1}{\partial y} = 0, & \text{at } y = 0.5. \end{cases} \end{aligned} \tag{43}$$

The solution to (43) is given by:

$$\zeta_1(y) = \frac{1}{2(1-\mathrm{e}^{\beta})}\mathrm{e}^{\beta y} + \frac{\mathrm{e}^{\beta}}{2(1-\mathrm{e}^{\beta})}\mathrm{e}^{-\beta y}. \tag{44}$$

From (35), (37) and (42), the velocity field is obtained as:

$$\begin{cases} u = 1 - \left(\dfrac{1}{(1-\mathrm{e}^{\beta})}\mathrm{e}^{\beta y} + \dfrac{\mathrm{e}^{\beta}}{(1-\mathrm{e}^{\beta})}\mathrm{e}^{-\beta y}\right)\varepsilon\beta\sin(\beta x) \\ v = \left(\dfrac{1}{(1-\mathrm{e}^{\beta})}\mathrm{e}^{\beta y} - \dfrac{\mathrm{e}^{\beta}}{(1-\mathrm{e}^{\beta})}\mathrm{e}^{-\beta y}\right)\varepsilon\beta\cos(\beta x). \end{cases} \tag{45}$$

Finally, the tortuosity is obtained by substituting (45) into (31), as:

$$\alpha_\infty = 1 + \frac{\mathrm{e}^{\beta}+1}{\mathrm{e}^{\beta}-1}\varepsilon^2\beta. \tag{46}$$

3.3. *Effective density and effective compressibility*

According to the semi-phenomenological model for porous media [2], the effective density ρ and the effective compressibility C of the present micro-slits with surface roughness can be obtained as:

$$\rho/\rho_0 = \alpha_\infty + \frac{\nu}{j\omega k_0}\left(1 - c + c\left[1 + \left(\frac{2\alpha_\infty k_0}{c\Lambda}\right)^2\frac{j\omega}{\nu}\right]^{1/2}\right) \tag{47}$$

$$C \times \gamma P_0 = \gamma - \frac{\gamma - 1}{1 + \frac{\nu'}{j\omega k_0'}\left[1 + \left(\frac{\Lambda'}{4}\right)^2\frac{j\omega}{\nu'}\right]^{1/2}}. \tag{48}$$

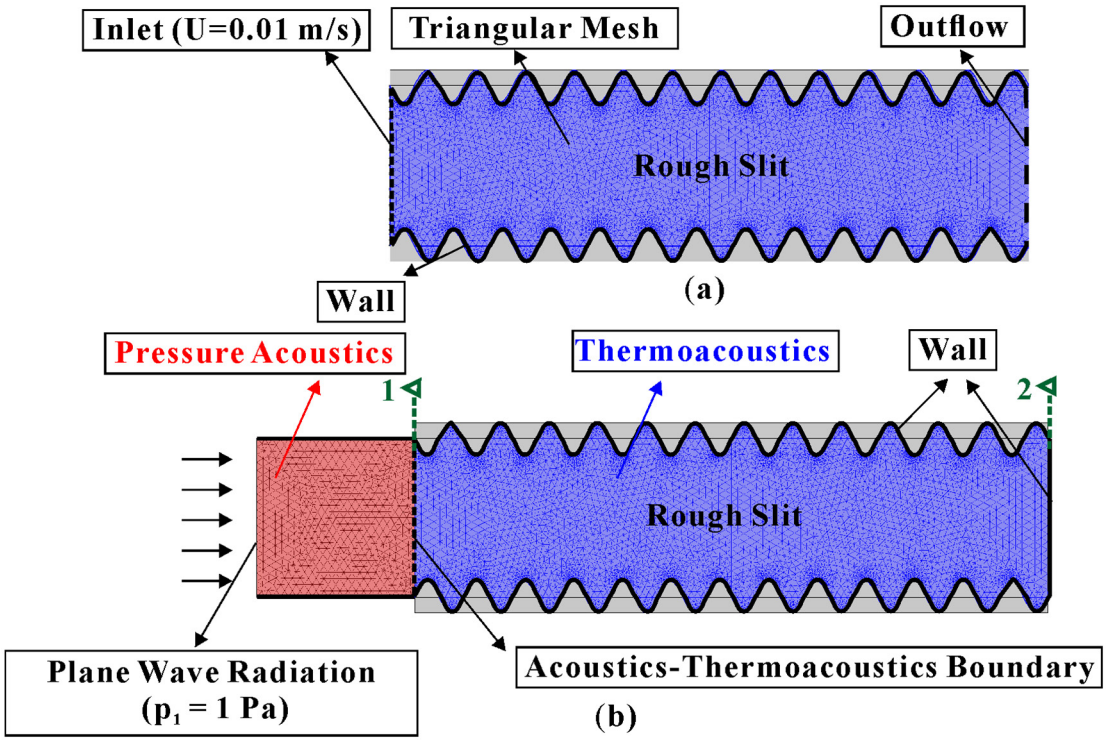

Figure 3. Finite element simulations: (a) computational domain for determining static flow resistivity; (b) computational domain for calculating the effective density and effective compressibility.

where $c = 5/6$ is given in micro slit, the remaining acoustic parameters are defined in table 1. Relevant environmental and material parameters are listed in table 2.

3.4. Extension to a porous medium containing parallel rough slits

The previous analysis of acoustic properties of a single rough slit can be extended to study porous media containing a series of parallel rough slits. Following the approach of Stinson and Champoux [9], consider an idealized porous material composed of parallel rough slits having identical width, length and surface geometry. Let the porosity of the material be represented by Ω, and the ratio of slit length to the length of the porous material by τ. Based on these definitions, the effective density and effective compressibility of the porous material can be obtained as $\rho_m = \rho\tau^2/\Omega$ and $C_m = C\Omega$. Accordingly, the characteristic impedance and wavenumber of the porous material are $Z_m = \sqrt{\rho_m/C_m}$ and $k_m = \omega\sqrt{\rho_m C_m}$.

In practice, the width of the pores in a porous material may be randomly distributed. Horoshenkov *et al* [12, 13] studied this problem by adopting a log-normal statistical distribution in porous media. Approximated solutions of the viscosity correction function were obtained and proved to be accurate in the whole frequency range. The current research on parallel rough slits may be extended to study porous media by using the same method.

4. Validation of analytical model with numerical simulation

FE simulations are performed to verify the proposed analytical model. Static flow resistivity determined in viscous fluid, tortuosity determined in non-viscous fluid as well as effective density and effective compressibility calculated in viscous sound field are obtained using COMSOL Multiphysics 5.0. The equations solved in the FE simulations are given in appendix B.

4.1. Static flow resistivity and tortuosity

According to figure 3(a), numerical simulations of steady viscous incompressible flow passing a rough micro-slit are carried out using the Creeping Flow Model of COMSOL. With the diameter of the slit fixed as 1 mm, its length is set sufficiently large to ensure at least four periods of wavy roughness in the direction of flow. All triangular elements are adopted to discretize the governing equations, with grid dependence carefully analyzed to ensure numerical convergence. The grid near the boundary has been refined automatically, based on the geometry of the wavy roughness. The inlet velocity is 0.01 m s^{-1}, while the outlet is set as Laminar Outflow. The remaining walls of the slit are all set as No Slip. Taking the two dimensional (2D) model of figure 3(a) into the Stationary Solver, one can finally obtain the velocity distribution in the fully developed range of flow. Subsequently, based on average velocity and pressure drop, the static flow resistivity is calculated by equation (2).

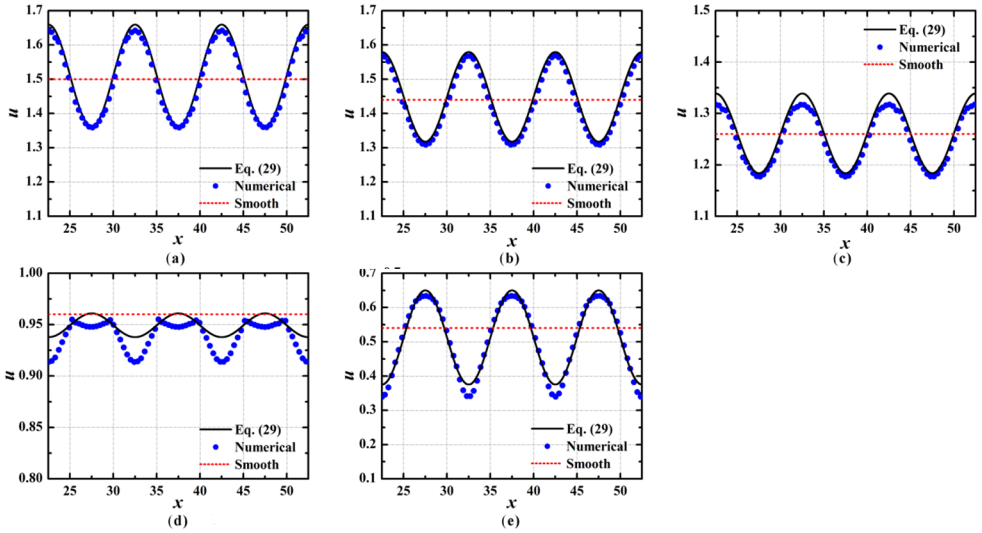

Figure 4. Theoretical model predictions compared with numerical simulation results for dimensionless flow velocity at selected heights of roughened micro-slit: (a) $y = 0.5$ (center line of channel), (b) $y = 0.4$, (c) $y = 0.3$; (d) $y = 0.2$ and (e) $y = 0.1$, for the case of $\varepsilon = 0.05$, $\beta = 0.2\pi$.

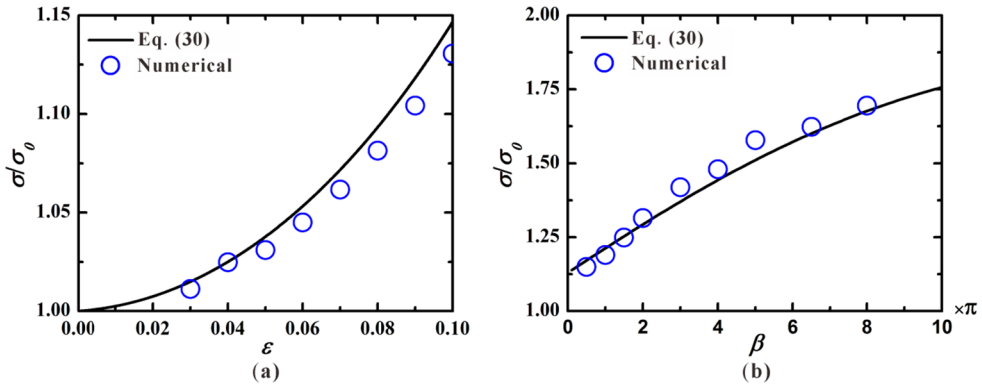

Figure 5. Comparison of theoretical predictions and numerical results on static flow resistivity: (a) influence of relative roughness ($a = 1$ mm, $\beta = 0.2\pi$); (b) influence of wave number of roughness ($a = 1$ mm, $\varepsilon = 0.1$).

Simulations of inviscid incompressible flow are performed with the Laminar Flow Model. Slip Boundary Condition ($\mathbf{u}\cdot\mathbf{n} = 0$) is adopted on slit wall and the dynamic viscosity of the fluid is set as zero. Once the flow filed is determined, the tortuosity is calculated by equation (31).

4.2. Effective density and effective compressibility

With reference to figure 3(b), FE simulations of viscous sound waves passing a rough micro-slit are performed using the 2D Acoustic-Thermoacoustic Interaction Model. Typically, the simulation model is consisted of two parts. The first is named as the 'input', i.e. red region of figure 3(b), where the Pressure-Acoustics Model (a physical model in COMSOL, where viscosity is ignored) is applied. Plane wave radiation generated in this domain propagates along the slit. The second is considered as the rough channel, i.e. blue region, where the Thermoacoustics Model (another physical model in COMSOL where thermal and viscous effects are both taken into consideration) is employed. Simulations of effective density and effective compressibility are performed in this domain. Both parts are meshed by triangular elements, with grid independence ensured before final calculation.

According to figure 3(b), the inlet of the first part is set as plane wave radiation perpendicular to the cross section of slit, while the outlet of the second part is set as Solid Wall. While the interface between the two parts are set as Acoustic-Thermoacoustic Boundary, the remaining boundaries are all set as Sound Hard Boundary (a boundary condition in COMSOL, which is assumed to be solid, no-slip and isothermal). The frequency range considered is $0 < f \leqslant 10^4$ Hz. Upon substituting the FE model to the Frequency Domain Solver, the sound field is obtained.

Based on the numerical results of sound field, the effective density and effective compressibility are determined with the transfer function method [17, 48]. Firstly, the surface impedance at the entrance of the rough slit (i.e. surface-1 in figure 3(b)) is calculated by $Z_s = \langle p\rangle_{in}/\langle v\rangle_{in}$, where $\langle p\rangle_{in}$ and $\langle v\rangle_{in}$ are the surface average of acoustic pressure and velocity at the entrance. Then, the transfer function of the acoustic system is given by $T = \langle p\rangle_{in}/\langle p\rangle_{out}$, where $\langle p\rangle_{out}$ is the surface average of acoustic pressure at the outlet (i.e. surface-2 in figure 3(b)). Therefore, the characteristic impedance and propagation constant can be calculated from $Z = Z_s\sqrt{(T^2-1)/T^2}$ and $\theta = \text{arccosh}(T)/jd$. Finally, based

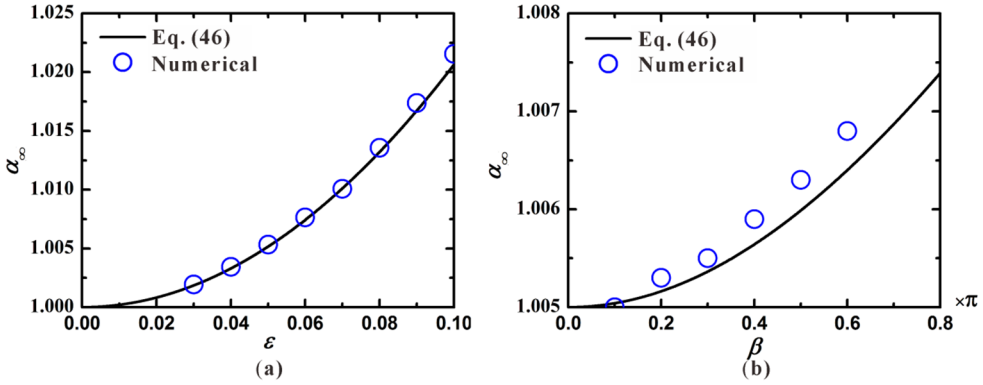

Figure 6. Comparisons of theoretical predictions and numerical results on tortuosity: (a) influence of relative roughness ($a = 1$ mm, $\beta = 0.2\pi$); (b) influence of wave number of roughness ($a = 1$ mm, $\varepsilon = 0.05$).

on the relations of $Z = \sqrt{(\rho/C)}$ and $\theta = \omega\sqrt{\rho C}$, the effective density and effective compressibility are obtained.

5. Results and discussion

5.1. Static flow resistivity

5.1.1. Velocity distribution in creeping flow. The influence of roughness on velocity distribution in static incompressible creeping flow is quantified, with reference to equation (29). For the case of $\varepsilon = 0.05$ and $\beta = 0.2\pi$, figure 4 compares theoretical model predictions with numerical simulation results for dimensionless velocity component u at selected channel heights ($y = 0.5$, 0.4, 0.3, 0.2, 0.1). Corresponding results of smooth slit are given as reference. The predictions match well with numerical results.

The results of figure 4 reveal two significant features of the flow field: one is periodic fluctuation with reference to equation (15), and the other is overall deviation with reference to equation (16). The periodic fluctuation represents the periodic variation of u, which exhibits the same period as the roughness. The phase of the periodic fluctuation depends on position (i.e. the value of y). As y is near the slit center line 0.5, u has the same phase as the roughness (figure 4(a)). In contrast, when y approaches $\varepsilon\cos(\beta x)$ near the roughened slit wall, u has a phase opposite to that of roughness (figure 4(e)). Consequently, when $y \in (\varepsilon\cos(\beta x), 0.5)$, there must exist a phase-change-line, where the phase of the periodic fluctuation changes (figure 4(d)). According to equation (29), the exact position of this phase-change-line can be calculated by solving the following equation:

$$e^{2\beta y_0} - e^{\beta} = \frac{2e^{\beta} + \beta e^{\beta} + e^{2\beta}\beta - 2e^{2\beta}}{(\beta e^{\beta} - \beta)y_0 + (e^{\beta} - 1 - e^{\beta}\beta)} \tag{49}$$

where $y = y_0$ is the phase-change-line, which is merely influenced by the wave number of the roughness. In addition, the amplitude of periodic variation depends on the position, highest near the center line and the boundary line, and lowest near the phase-change-line. Although the average amplitude of the periodic variation is considerably large relative to the average velocity, it has little contribution to the growth of pressure drop across the slit, due mainly to the following integral properties of the trigonometric function:

$$\int_0^{2\pi/\beta} [\varphi_1(y)e^{j\beta x} + \varphi_{-1}(y)e^{-j\beta x}]\,dx = 0. \tag{50}$$

Overall deviation represents the overall variation of average velocity v along y direction. It quantifies the difference between the symmetrical axis of the periodic variation and the velocity with the smooth slit serving as reference (i.e. red dot line in figure 4). The results of figures 4(a)–(c) show that the difference is small enough to be neglected. In comparison, visible difference between figures 4(d) and (e) can be found. In most cases, the difference can be neglected without loss of accuracy [41]. However, in the present problem, overall deviation is critical [42]. From the view point of fluid dynamics, the resistance of surface roughness leads to flow concentration near the center line (i.e. overall deviation), thus reducing the hydraulic radius. According to $\sigma_0 = 3\mu/a^2$, decreasing hydraulic radius increases static flow resistivity. On the other hand, pressure drop is the second-order derivative of velocity. Mathematically speaking, the magnitude of a second-order derivative is irrelevant to the magnitude of its original function. Although the overall deviation of flow velocity is so small that it can be neglected, the corresponding increase in pressure drop can be large, as illustrated in the following section.

5.1.2. Static flow resistivity. The influence of wavy roughness on static flow resistivity is investigated. To eliminate the influence of geometric scale, the static flow resistivity σ in a rough slit is normalized by σ_0 in the reference smooth slit. To validate the proposed model of equation (30), comparisons between analytical predictions and numerical results are made. Each blue symbol in the figure represents the static flow resistivity of a particular kind of micro rough slit, which has been simulated independently. The calculation error of different simulations may lead to the lack of smoothness in the numerical results, which can be improved by refining the grid. As shown in figure 5(a) for the case of $a = 1$ mm and $\beta = 0.2\pi$. Figure 5(b) for the case of $a = 1$ mm and $\varepsilon = 0.1$, good agreement is achieved. The static flow resistivity is significantly affected by the presence of surface roughness.

According to figure 5(a), increasing relative roughness not only causes the static flow resistivity to grow but also increases the rate of growth. While the lower limit is given by $\sigma/\sigma_0 = 1$ when $\varepsilon = 0$. However, there is no upper limit.

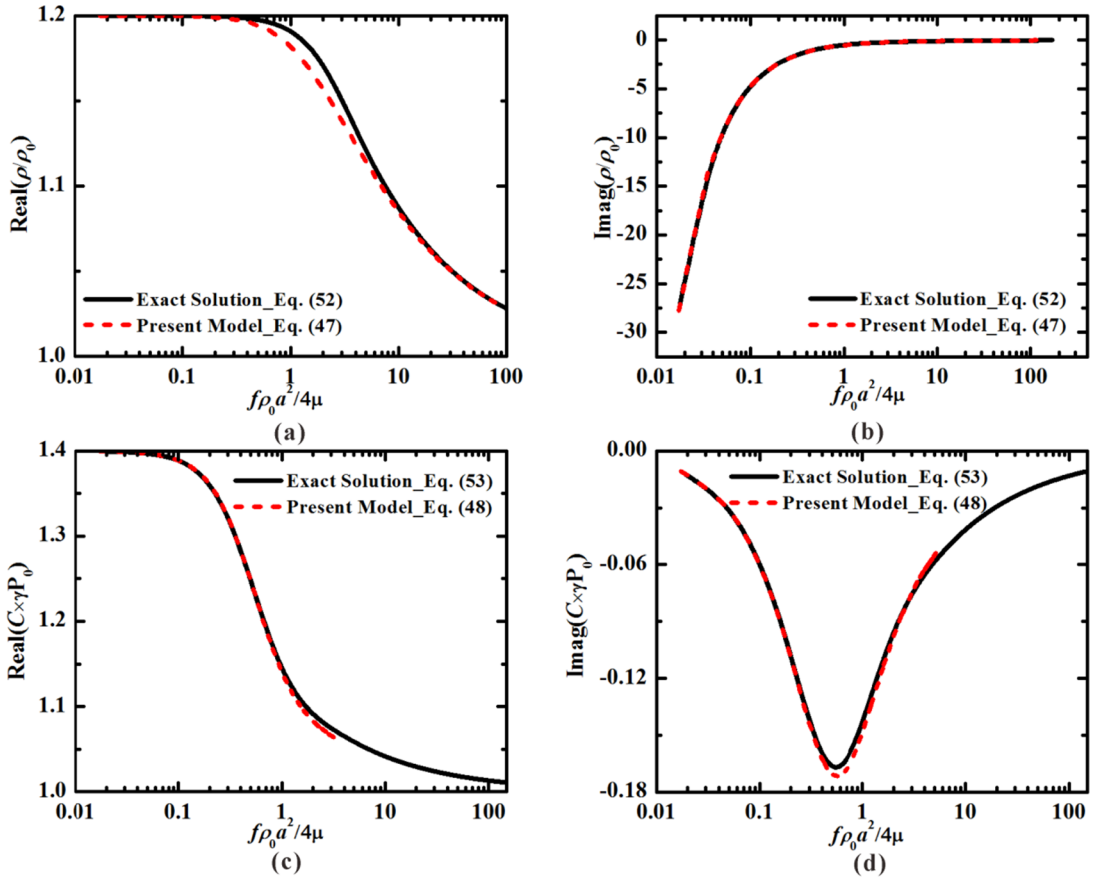

Figure 7. The exact solutions (i.e. equations (52) and (53)) compared with the present model (i.e. equations (47) and (48)) for normalized effective density and normalized effective compressibility ($a = 1$ mm, $d = 50$ mm): (a) real part of effective density; (b) imaginary part of effective density; (c) real part of effective compressibility; (d) imaginary part of effective compressibility.

The static flow resistivity increases with increasing wave number of roughness, but with decreasing growth rate; figure 5(b). The lower limit is given by $\sigma/\sigma_0 = (2\varepsilon^2 + 1)/(1 - 4\varepsilon^2)^{2.5}$ at $\beta \to 0$, and the upper limit is given by $\sigma/\sigma_0 = (1 - 2\varepsilon)^{-3}$ at $\beta \to \infty$. The difference between the lower and upper limits is huge, which demonstrates that the static flow resistivity is critically dependent upon the distribution density of roughness.

The growth of static flow resistivity with increasing roughness can be reasoned by the reduction of hydraulic radius. The presence of surface roughness increases the perimeter of slit boundary, but does not change the cross-sectional area, resulting in smaller hydraulic radius and thence higher viscous stress. According to equation (29), the period average of the increase in viscous stress, which can be calculated by $\frac{\beta}{2\pi}\int_0^{2\pi/\beta} \nabla u_1 \mathrm{d}x$, is the largest on the slit boundary and smallest at the center line. As a result, the flow rate near the center line is larger than that near the boundary, which leads to the overall deviation of the flow field detailed in section 5.1.

5.2. Tortuosity

This section aims to evaluate analytically the influence of wavy roughness on tortuosity, with corresponding numerical simulation results given for comparison. Figure 6(a) displays the influence of relative roughness for the case of $a = 1$ mm, $\beta = 0.2\pi$, while figure 6(b) displays the influence of wave number of roughness for the case of $a = 1$ mm, $\varepsilon = 0.05$. In a smooth slit, $\alpha_\infty = 1$. In both cases, the agreement between analytical prediction and numerical simulation is good.

It is seen from figure 6 that the tortuosity increases monotonically with relative roughness and a lower limit is found when $\varepsilon \to 0$. Increasing the wave number of roughness also causes significant increase in tortuosity, and there is a lower limit given by $\alpha_\infty = 1 + 2\varepsilon^2$ when $\beta \to 0$. For both cases, no upper limit is found. In fact, equation (46) is reliable only when $\beta \ll 2\pi/\varepsilon$. As verification, the lower limit predicted using an alternative method [2] is provided here. When $\beta \to 0$, the flow field is evenly distributed in the rough slit, which can be equivalent to a series of smooth slits. Thus the velocity components can be approximated by $u(x, y) = \frac{1}{1 - 2\varepsilon\sin(\beta x)}$ and $v(x, y) = 0$ which, together with equation (31), leads to $\alpha'_\infty\big|_{\beta\to 0} = 1/\sqrt{1 - 4\varepsilon^2}$. The difference between the two lower limits of tortuosity is:

$$\alpha'_\infty\big|_{\beta\to 0} - \alpha_\infty\big|_{\beta\to 0} = (1 - 4\varepsilon^2)^{-0.5} - (1 + 2\varepsilon^2) = o(\varepsilon^2) \quad (51)$$

which demonstrates that the proposed expression of tortuosity has considerable accuracy near the lower limit.

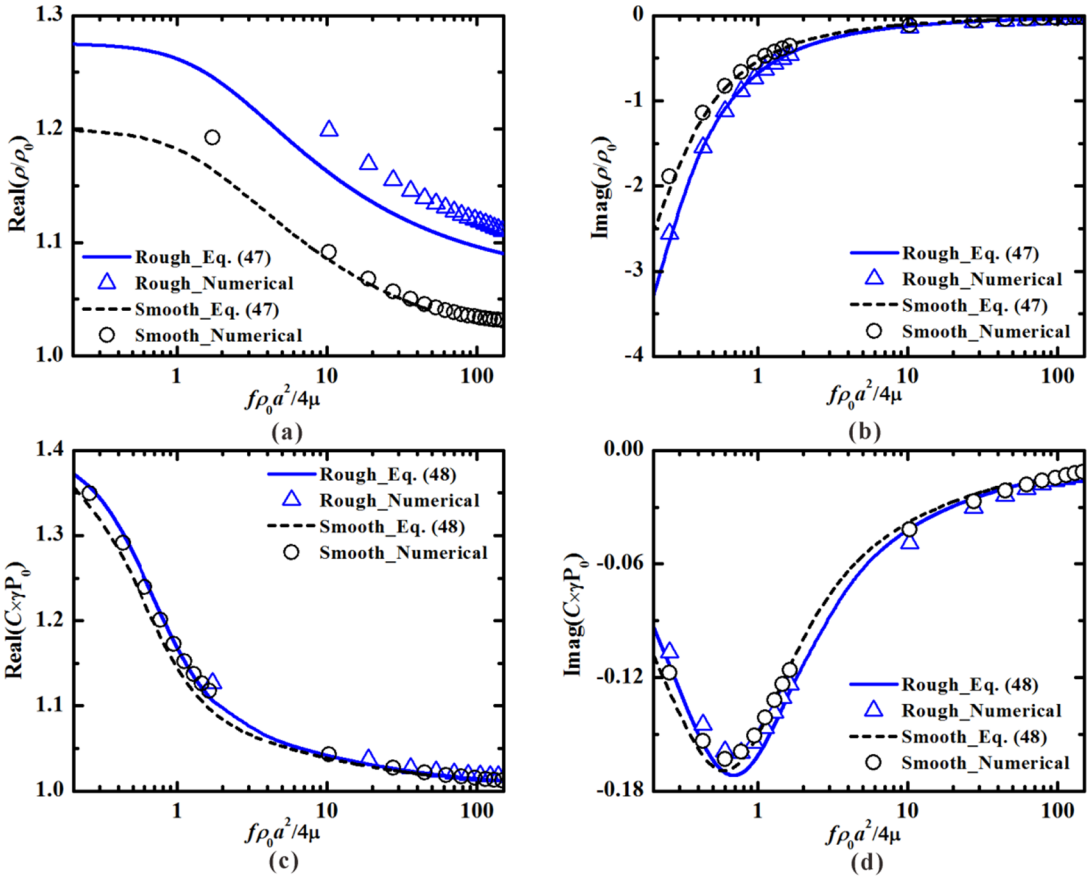

Figure 8. Comparisons of analytical predictions and numerical results on normalized effective density and normalized effective compressibility ($a = 1\,\text{mm}$, $d = 50\,\text{mm}$, $\beta = 2\pi$ and $\varepsilon = 0.1$): (a) real part of effective density; (b) imaginary part of effective density; (c) real part of effective compressibility; (d) imaginary part of effective compressibility.

The increase of tortuosity depends in general on the slope of the boundary function characterizing the roughened slit surface. In fact, the wavy slit boundary changes flow direction on the boundary, which is passed to the whole flow field without decay (i.e. without viscous dissipation). As a result, the change of flow direction causes diffusion of the flow field, increasing thus the tortuosity.

5.3. Effective density and effective compressibility

For a better comparison, let the frequency be normalized by $f' = \left(\frac{f\rho_0 a^2}{4\mu}\right)$, the effective density be normalized by ρ/ρ_0 and the effective compressibility be normalized by $C \times \gamma P_0$. Since equations (47) and (48) are approximated solutions of the sound field of a micro-slit, their accuracy needs to be checked. The exact solutions of effective density and effective compressibility of a slit in the limit of zero roughness are given by [9]:

$$\rho/\rho_0 = 1 \Bigg/ \left[1 - \frac{\tanh\left(s\sqrt{j}\right)}{s\sqrt{j}}\right] \tag{52}$$

$$C \times \gamma P_0 = 1 + (\gamma - 1)\frac{\tanh\left(\sqrt{\text{Pr}}\, s\sqrt{j}\right)}{\sqrt{\text{Pr}}\, s\sqrt{j}} \tag{53}$$

where $s = \sqrt{\omega\rho_0 a^2/4\mu}$. Figure 7 compares the exact solutions, i.e. equations (52) and (53), of normalized effective density and normalized effective compressibility with the present approximated solutions, i.e. equations (47) and (48). The results demonstrate that, in the limit of zero-roughness, the approximated solutions do approach the exact solutions in the whole frequency range considered. The maximum relative deviation is less than 1%.

Figure 8 plot the effective density and effective compressibility as functions of dimensionless frequency, f', with corresponding results for smooth slit included as reference. Without loss of generality, relevant geometrical parameters are given by $a = 1\,\text{mm}$, $d = 50\,\text{mm}$, $\beta = 2\pi$ and $\varepsilon = 0.1$. Figure 8(a) reveals a significant increase in the real part of effective density in a rough micro-slit relative to that of a smooth one. The increment remains unchanged in the whole frequency range considered. Based on figure 8(b), while the increase in the imaginary part of effective density is significant at relatively low frequencies, it gradually vanishes as the frequency is increased. These limiting properties of the effective density can be elaborated using the present analytical model, as illustrated below.

In the low frequency range, the effective density has a first-order approximation in angular frequency ω given by:

$$\rho(\omega) = \alpha_0\rho_0 - \frac{\sigma}{\omega}j \tag{54}$$

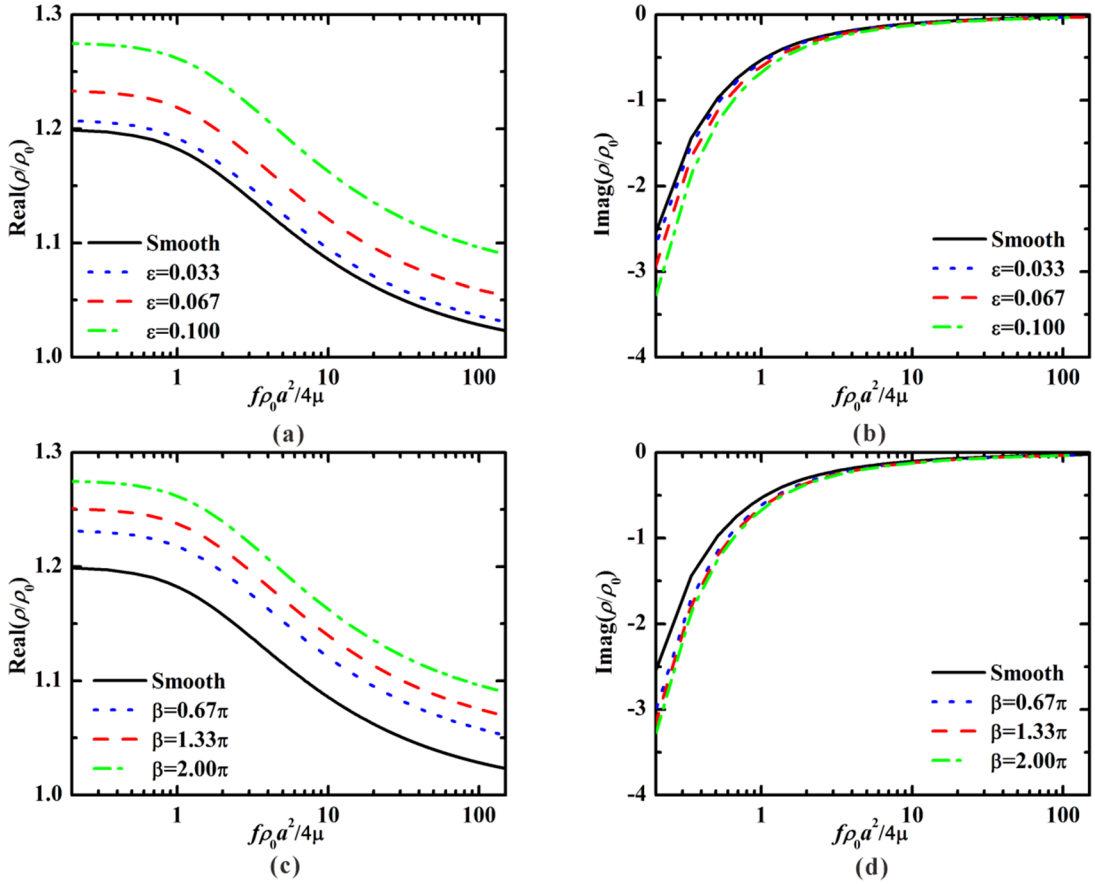

Figure 9. Predicted roughness effect on normalized effective density: (a) influence of relative roughness on the real part ($a = 1$ mm, $\beta = 2\pi$); (b) influence of relative roughness on the imaginary part ($a = 1$ mm, $\beta = 2\pi$); (c) influence of wave number of roughness on the real part ($a = 1$ mm, $\varepsilon = 0.1$); (d) influence of wave number of roughness on the imaginary part ($a = 1$ mm, $\varepsilon = 0.1$).

while, in the high frequency range, it has a first-order approximation in $1/\sqrt{\omega}$ as:

$$\rho(\omega) = \alpha_\infty \rho_0 \left[1 + (1-j)\frac{1}{\Lambda}\sqrt{\frac{2\mu}{\omega\rho_0}}\right]. \tag{55}$$

For the real part, $\lim_{\omega\to 0}\text{Real}(\rho/\rho_0) = \alpha_0 \approx 1.2\alpha_\infty$ and $\lim_{\omega\to\infty}\text{Real}(\rho/\rho_0) = \alpha_\infty$. As the real part of effective density is proportional to tortuosity, the increase in tortuosity can definitely lead to increase in the real part of effective density in the whole frequency range. It also means that the relative error of the real part of effective density can be approximated by the relative error of the tortuosity, which accounts for the minor deviation (around 10%) between the theoretical predictions and numerical results in figure 7(a).

For the imaginary part, $\lim_{\omega\to 0}\text{Imag}(\rho/\rho_0) = -\sigma/\omega$ and $\lim_{\omega\to\infty}\text{Imag}(\rho/\rho_0) = -\frac{j}{\Lambda}\sqrt{\frac{2\mu}{\omega\rho_0}}\alpha_\infty$. The lower limit is infinite and the upper limit is zero. Clearly, in the low frequency range, the convergence rate of the imaginary part is proportional to static flow resistivity. Consequently, in the low frequency range, it is the increase in static flow resistivity that causes the growth of the imaginary part of effective density.

As concerning the effective compressibility, according to figures 8(c) and (d), there is no obvious difference between rough and smooth micro-slits. In other words, roughness has little effect on the thermal properties of the slit. In fact, the lower limit of the normalized effective compressibility is $C \times \gamma P_0 = \gamma - \omega j\frac{\Lambda'^2}{12}\frac{\gamma-1}{\nu'}$ when $\omega \to 0$ and the upper limit is $C \times \gamma P_0 = 1 + (\gamma-1)\frac{3}{\Lambda'}\sqrt{\frac{\nu'}{\omega}}\left(\frac{\sqrt{2}}{2} - \frac{\sqrt{2}}{2}j\right)$ when $\omega \to \infty$. The influence of roughness, decided by Λ', only appears in the infinite term. Given that equation (48) critically depends on the characteristics of these limitations, roughness may have little influence on the thermal properties of the micro-slit.

Figure 9 provides more details concerning the effect of roughness on effective density. The influence of relative roughness is illustrated in figures 9(a) and (b) for the case of $a = 1$ mm, $\beta = 2\pi$. The influence of wave number of roughness is illustrated in figures 9(c) and (d) for the case of $a = 1$ mm, $\varepsilon = 0.1$. According to the results presented in sections 5.1 and 5.2, both the relative roughness and wave number of roughness can lead to the growth of static flow resistivity and tortuosity. Such growth increases the effective density as well, as shown explicitly in equations (54) and (55).

6. Conclusion

An analytical model for the influence of wavy surface roughness on the acoustic properties of micro-slits is established. Small parameter analysis is performed by assuming that the roughness has relatively small amplitude compared to slit

opening. Finite element simulations are performed to validate the proposed model, with good agreement achieved. The main conclusions drawn are as follows:

(i) For static creeping flow, the variation of flow velocity follows a trigonometric pattern, where the periodic fluctuation dictates the period, phase and amplitude, while the overall deviation determines the symmetrical line. The static flow resistivity of the micro-slit increases significantly with increasing relative roughness or wave number of roughness or both.
(ii) Increasing the relative roughness or wave number of roughness increases the tortuosity of the micro-slit. The extent to which the tortuosity is increased depends on the slope of the boundary function that characterizes the roughened slit surface.
(iii) The presence of wavy roughness increases the effective density of the micro-slit, with its real part determined by tortuosity and its imaginary part by static flow resistivity, but has little effect on the effective compressibility.

It should be noted that there are some limitations of the current research: (i) the solutions can only be applied to the study of rough micro-slits; (ii) the Reynolds number must be small to ensure the inertial effect can be neglected; (iii) the wavelength of the roughness should be large enough to avoid a big slope on the boundary; (iv) only wavy roughness has been taken into consideration. These problems need to be further studied in future research. Nevertheless, the proposed approximated solution is accurate enough to be applicable in the design of micro-slit panels and other relevant acoustic structures. And the given perturbation method can be applied to the study of other kinds of rough micro-channels with different cross sections.

Acknowledgments

This work was supported financially by the National Natural Science Foundation of China (51528501 and 51506160), the China Post-Doctoral Science Foundation Project (2015M580845, 2016T90916), Shaanxi Province Post-Doctoral Science Foundation Project (2016BSHYDZZ54) and the Fundamental Research Funds for Central Universities (2014qngz12, xjj2016042).

Appendix A. Non-dimensional treatment

With references to figures 1 and 2, for low Reynolds number flow, take a as the reference length, U as the reference velocity, and $\mu U/a$ as the reference pressure [49]. Then,

$$x = \frac{\overline{x}}{a},\ \mathrm{y} = \frac{\overline{y}}{a},\ \mathbf{u} = \frac{\overline{\mathbf{u}}}{U},\ p = \frac{\overline{p}}{\mu U/a},\ \nabla = \frac{1}{a}\overline{\nabla} \tag{A.1}$$

where (x, y), $\mathbf{u}$, p and ∇ are separately the coordinates, velocity vector, pressure and gradient operator in dimensionless form, while $(\overline{x}, \overline{y})$, $\overline{\mathbf{u}}$, $\overline{p}$ and $\overline{\nabla}$ are the corresponding variables in dimensional form. Accordingly, the dimensionless Navior–Stokes equation is given by:

$$\mathrm{Re}\cdot(\mathbf{u}\cdot\nabla)\,\mathbf{u} = -\nabla p + \nabla^2\mathbf{u} \tag{A.2}$$

where Re is the Reynolds number defined by $\mathrm{Re} = \frac{\rho_0 U a}{\mu}$. When Re is infinitely large, equation (A.2) is reduced to equation (3).

Appendix B. The equations solved in the FE simulations

In the current research, all the numerical simulations are performed by finite element method embedded in COMSOL_Multiphysics_5.0.

Numerical simulations of steady viscous incompressible flow passing a rough micro-slit are carried out using the Creeping Flow Model of COMSOL. The equation solved in Creeping Flow Model is given by

$$\begin{aligned} 0 &= \nabla\cdot\left[-p\,\mathbf{I} + \mu(\nabla\,\mathbf{u} + (\nabla\mathbf{u})^T) - \frac{2}{3}\mu(\nabla\cdot\,\mathbf{u})\mathbf{I}\right] + \mathbf{F} \\ \nabla\cdot(\rho_0\mathbf{u}) &= 0 \end{aligned} \tag{B.1}$$

where F is the volume force.

Numerical simulations of inviscid incompressible flow are performed with the Laminar Flow Model of COMSOL. The equation solved in Laminar Flow Model is given by

$$\begin{aligned} \rho_0(\mathbf{u}\cdot\nabla)\,\mathbf{u} &= \nabla\cdot\left[-p\,\mathbf{I} + \mu(\nabla\,\mathbf{u} + (\nabla\mathbf{u})^T) - \frac{2}{3}\mu(\nabla\cdot\,\mathbf{u})\mathbf{I}\right] + \mathbf{F} \\ \nabla\cdot(\rho_0\mathbf{u}) &= 0. \end{aligned} \tag{B.2}$$

Numerical simulations of viscous sound wave passing a rough micro-slit are performed using the 2D Acoustic-Thermoacoustic Interaction Model. The equation solved in Pressure Acoustic Model is given by

$$\nabla\cdot\left(-\frac{1}{\rho_0}\right)(\nabla p_t - \mathbf{q}_\mathrm{d}) - \frac{[(\omega/c_0)^2 - k_z^2]\,p_t}{\rho_0} = Q_\mathrm{m} \tag{B.3}$$

where p_t is the acoustic pressure, Q_m is the monopole source, q_d is the dipole source, k_z is the wave number of the fluid, c_0 is the speed of sound.

The equation solved in Thermoacoustics Model is given by

$$\begin{aligned} \mathrm{i}\omega\rho_0\,\mathbf{u} &= \nabla\cdot\left[-p\,\mathbf{I} + \mu(\nabla\,\mathbf{u} + (\nabla\mathbf{u})^T) - \left(\frac{2}{3}\mu - \mu_\mathrm{B}\right)(\nabla\cdot\,\mathbf{u})\mathbf{I}\right] \\ \mathrm{i}\omega\rho + \rho_0\nabla\cdot\mathbf{u} &= 0 \\ \mathrm{i}\omega\rho_0 c_\mathrm{p} T &= -\nabla\cdot(-k\nabla T) + \mathrm{i}\omega\alpha_0 T_0 p + Q \end{aligned} \tag{B.4}$$

where μ_B is the bulk viscosity, c_p is the heat capacity at constant pressure, T_0 is the equilibrium temperature, T is the temperature, α_0 is the coefficient of thermal expansion (isobaric), Q is the heat source.

These models are carefully introduced in the help files of COMSOL.

References

[1] Smits J M A and Kosten C W 1951 *Acta. Acust.* **1** 114
[2] Allard J F and Atalla N 2009 *Propagation of Sound in Porous Media* (Singapore: Mrakono Print Media) p 90
[3] Zhang Q C *et al* 2015 *Prog. Mater. Sci.* **74** 332

[4] Maa D Y 2001 *Chin. J. Acoust.* **20** 1
[5] Allam S and Åbom M 2011 *J. Vib. Acoust.* **133** 031005
[6] Bravo T, Maury C and Pinhède C 2014 *Appl. Acoust.* **79** 47
[7] Xi Q, Choy Y S, Cheng L and Tang S K 2015 *J. Sound Vib.* **362** 39
[8] Rayleigh B and Strutt J W 1896 *The Theory of Sound* 2nd edn (London: Macmillan) p 317
[9] Stinson M R and Champoux Y 1992 *J. Acoust. Soc. Am.* **91** 685
[10] Johnson D L, Koplik J and Dashen R 1987 *J. Fluid Mech.* **176** 379
[11] Champoux Y and Allard J F 1991 *J. Appl. Phys.* **70** 1975
[12] Horoshenkov K V, Attenborough K and Chandler-Wilde S N 1998 *J. Acoust. Soc. Am.* **104** 1198
[13] Horoshenkov K V, Groby J-P and Dazel O 2016 *J. Acoust. Soc. Am.* **139** 2463
[14] Denayer H, Tournadre J, De Roeck W, Desmet W and Martinez-Lera P 2014 Combined numerical and experimental study of a slit resonator under grazing flow *Proc. 20th AIAA/CEAS Aeroacoustics Conf. (Atlanta, GA, USA)* (https://doi.org/10.2514/6.2014-2959)
[15] Ruiz H, Claeys C, Deckers E and Desmet W 2016 *Mech. Syst. Signal Process.* **70–1** 904
[16] Ruiz H, Claeys C C, Deckers E and Desmet W 2015 On the acoustic absorption of micro slitted metamaterials: a numerical and experimental study *Proc. 22nd Int. Congress on Sound and Vibration (Florence, Italy)*
[17] Ren S W, Meng H, Xin F X and Lu T J 2016 *J. Appl. Phys.* **119** 014901
[18] Dowling A P and Hughes I J 1992 *J. Sound Vib.* **156** 387
[19] Uris A, Bravo J M, Llinares J and Estelles H 2004 *Appl. Acoust.* **65** 421
[20] Taylor J B, Carrano A L and Kandlikar S G 2006 *Int. J. Therm. Sci.* **45** 962
[21] Darcy H 1857 *Recherches Expérimentales Relatives au Mouvement de L'Eau dans les Tuyaux* (Paris: Mallet-Bachelier)
[22] Mises R V 1915 *Mon.hefte Math. Phys.* **26** A27
[23] Nikuradse J 1950 Laws of flow in rough pipes *National Advisory Committee for Aeronautics Technical Report* 1292
[24] Colebrook C F and White C M 1937 *Proc. R. Soc. Lond.* A **161** 367
[25] Colebrook C F 1939 *J. Ice* **11** 133
[26] Moody L F 1944 *Trans. ASME* **66** 671
[27] Zou J and Peng X-F 2006 Effects of roughness on liquid flow behavior in ducts *United States: 2006 ASME Joint US—European Fluids Engineering Summer Meeting* (https://doi.org/10.1115/fedsm2006-98143)
[28] Mala G M and Li D 1999 *Int. J. Heat Fluid Flow* **20** 142
[29] Kandlikar S G, Schmitt D, Carrano A L and Taylor J B 2005 *Phys. Fluids* **17** 100606
[30] Wagner R N and Kandlikar S G 2012 *Heat Transfer Eng.* **33** 483
[31] Ning J F, Ren S W and Zhao G P 2016 *Appl. Acoust.* **111** 135
[32] Cortis A, Smeulders D M J, Guermond J L and Lafarge D 2003 *Phys. Fluids* **15** 1766
[33] Achdou Y and Avellaneda M 1992 *Phys. Fluids* A **4** 2651
[34] Meng H, Yang X H, Ren S W, Xin F X and Lu T J 2016 *Compos. Sci. Technol.* **127** 158
[35] Bashir I, Taherzadeh S and Attenborough K 2013 *J. Acoust. Soc. Am.* **134** 4691
[36] Ingard U 1953 *J. Acoust. Soc. Am.* **25** 1037
[37] Lessen M and Huang P-S 1976 *Phys. Fluids* **19** 945
[38] Pozrikidis C 1987 *J. Fluid Mech.* **180** 495
[39] Munson B R, Rangwalla A A and Mann J A 1985 *Phys. Fluids* **28** 2679
[40] Dyke M V 1964 *Perturbation Methods in Fluid Mechanics* (Stanford, CA: Parabolic) pp 36–7
[41] Wang H, Wang Y and Zhang J 2005 *J. Fluids Eng.* **127** 1140
[42] Wang C Y 1978 *Phys. Fluids* **21** 697
[43] Chu Z K-H 2000 *J. Phys. D: Appl. Phys.* **33** 627
[44] Si D and Jian Y 2015 *J. Phys. D: Appl. Phys.* **48** 085501
[45] ASTM 2009 C522-03, Standard Test Method for Airflow Resistance of Acoustical Materials
[46] Gershenfeld N 2011 *The Nature of Mathematical Modeling* (Cambridge: Cambridge University Press)
[47] Hosmer D W and Lemesbow S 2000 *Applied Logistic Regression* 2nd edn (New York: Wiley) pp 7–11
[48] Champoux Y and Stinson M R 1991 *J. Acoust. Soc. Am.* **90** 2182
[49] Li X Y, Ren S C and He Q C 2015 *Acta Mech. Sin.* **31** 32